

The disk reverberation mapping of X-ray weak quasars: a case study of SDSS J153913.47+395423.4

MARCIN MARCULEWICZ ¹, MOUYUAN SUN ¹, JIANFENG WU ¹ AND ZHIXIANG ZHANG ¹

¹*Department of Astronomy, Xiamen University, Xiamen, Fujian 361005, People's Republic of China*

(Received X, 2023; Revised X, 2023; Accepted X, 2023)

ABSTRACT

The widely adopted “lamppost” thermal reprocessing model, in which the variable UV/optical emission is a result of the accretion disk reprocessing of the highly fluctuating X-ray emission, can be tested by measuring inter-band time lags in quasars spanning a range of X-ray power. This work reports the inter-band time lag in an apparently X-ray weak quasar, SDSS J153913.47+395423.4. A significant cross-correlation with a time delay of ~ 33 days (observed-frame) is detected in the Zwicky Transient Facility (ZTF) g and r light curves of SDSS J153913.47+395423.4. The observed X-ray power seems to be too weak to account for the observed inter-band cross-correlation with time delay. Hence the X-ray weak quasar SDSS J153913.47+395423.4 is either intrinsically X-ray normal (but observationally X-ray weak), or the X-ray emission is not the only mechanism to drive UV/optical variability. In the former case, the required X-ray power is at least 19 times stronger than observed, which requires either an exceptionally anisotropic corona or Compton-thick obscuration. Alternatively, the Corona-heated Accretion disk Reprocessing (CHAR) or the EUV torus models may account for the observed time lags.

Keywords: Supermassive black holes (1663); Quasars (1319); Active galactic nuclei (16); Accretion (14)

1. INTRODUCTION

The central engine of Active Galactic Nuclei (AGNs), which are powered by accretion of gas onto supermassive black holes (SMBHs), generally is too compact to be spatially resolved and can only be probed in the time or spectral domains. One popular method is disk reverberation mapping, which measures the inter-band time delays of AGN disk continua. The standard thin disk model predicts that the emission-region size scales as $R \propto \lambda^{4/3}$ (Shakura & Sunyaev 1973), where R is the characteristic radius of the emission at a given wavelength (λ). The observed inter-band cross-correlation indicates that the same physical mechanism likely drives the variations in different emission regions. The observed time delays are from hours to days (e.g., Fausnaugh et al. 2016; McHardy et al. 2018; Cackett et al. 2020, 2021; Guo, H. et al. 2022; Guo, W.-J. et al. 2022). Hence, the time delays are not connected with the radial viscous propagation timescale (i.e., the viscous timescale of a geometrically-thin disk) since this timescale in UV/optical emission regions is longer than ~ 100 years. Instead, the radial propagation velocity of the driving mechanism should be close to the speed of light (Krolik et al. 1991). One possible driving mechanism is “lamppost” thermal reprocessing (e.g., Cackett et al. 2007). In this model, the X-ray corona acts as a lamppost and illuminates the accretion disk. The disk absorbs a fraction of the illuminated fluctuating X-ray power and reprocesses it as variable UV/optical thermal emission. Hence, the measured inter-band time delays are the light travel time to various emission regions.

The disk reverberation-mapping method can test the “lamppost” thermal reprocessing model. Indeed, inter-band time delays have been measured for some AGNs spanning a range of luminosity or black-hole mass (e.g., Fausnaugh

et al. 2016; McHardy et al. 2018; Homayouni et al. 2019; Guo, H. et al. 2022; Guo, W.-J. et al. 2022). Interestingly, the time delays are not entirely consistent with the X-ray reprocessing of the Shakura & Sunyaev disk (Shakura & Sunyaev 1973).

There are several studies that have tackled the "time lag discrepancy issue". For instance, disk winds can flatten the disk temperature profile (Sun et al. 2019) or create a rimmed and rippled accretion disk (Starkey et al. 2023); the disk emission is non-blackbody (Hall et al. 2018); there is a diffuse continuum from extended broad-line regions (e.g., Cackett et al. 2018; Korista & Goad 2019); coronae can have large scale heights (Kammoun et al. 2021b); time lags are not the light travel time (Cai et al. 2018; Sun et al. 2020).

From the theoretical point of view, the "lamppost" thermal reprocessing model has a long-standing energy budget problem (e.g., Clavel et al. 1992; Dexter et al. 2019). It is well known that the ratio of the X-ray emission at 2 keV to the UV emission at 2500 Å decreases with increasing UV luminosity (see, e.g., Just et al. 2007; Lusso et al. 2010). Hence, while the X-ray illumination might be powerful enough to drive the observed UV/optical variability in low-luminosity AGNs, the same process should be inefficient in luminous quasars. The X-ray weakness of a quasar can be described by the relative power of the X-ray and UV emission α_{OX} , which is the ratio of the monochromatic flux density at rest-frame 2 keV to that at rest-frame 2500 Å, i.e., $\alpha_{\text{OX}} = 0.3838 \log(L_{2\text{keV}}/L_{2500\text{Å}})$ (Tananbaum et al. 1979). The relation between α_{OX} and L_{2500} (e.g., Just et al. 2007; Lusso et al. 2010; Timlin et al. 2020) can be seen in Fig. 1. For normal AGNs, α_{OX} is highly correlated with L_{2500} (see the right panel of Fig. 1). For very luminous quasars, the X-ray emission can be much weaker than the UV/optical one. The same issue has been found in Seyferts by previous works (e.g., Uttley et al. 2003; Arévalo et al. 2008) which showed that, on longer timescales, the optical variability is too large to be driven by the thermal reprocessing.

The energy-budget problem is even more challenging in X-ray weak quasars, a special class of quasars that produce much less X-ray emission than expected from the $\alpha_{\text{OX}}-L_{2500}$ relation. A useful parameter is $\Delta\alpha_{\text{OX}}$, which measures the difference between the observed α_{OX} and expected α_{OX} from the $\alpha_{\text{OX}} - L_{2500}$ relation (e.g., Gibson et al. 2008; Wu et al. 2012). At rest-frame 2 keV, $\Delta\alpha_{\text{OX}} = -0.38$ corresponds to an X-ray weakness of factor 10. X-ray weak quasars can have $\Delta\alpha_{\text{OX}}$ of ~ -0.43 (e.g., Ni et al. 2018, 2022), and even up to -0.81 for PHL 1811 (Wang et al. 2022). The remarkable population of weak-line quasars has a typical equivalent width value of the C IV emission line ≤ 10 Å (e.g. Diamond-Stanic et al. 2009; Wu et al. 2012). Nearly half of the weak-line quasars are also X-ray weak (e.g. Wu et al. 2011, 2012; Ni et al. 2018; Marlar et al. 2018).

There are two physical explanations for their X-ray weakness. First, the X-ray weakness is caused by the intrinsic properties of the corona, which is unable to generate X-ray emission efficiently (e.g. Miniutti et al. 2012). Second, the apparent X-ray weakness is caused by strong gas obscuration due to some "shielding" gas (e.g., the accretion disk, disk wind, and the broad line region (BLR) clouds; see, e.g., Murray et al. 1995; Proga et al. 2000; Wu et al. 2011, 2012). Recent results amplify the idea of external absorption caused by winds (Wang et al. 2022) that prevent the observer and the BLR from receiving the X-ray emission. For instance, according to the measured X-ray stacked analysis of X-ray weak quasars (Luo et al. 2015; Ni et al. 2018, 2022) the observed X-ray weakness may have originated in heavy absorption due to small-scale shielding. The hard X-ray spectra show average effective power-law photon indices of $\sim 1.2-1.4$. These values suggest high levels of intrinsic X-ray absorption of $N_{\text{H}} \geq 10^{23} \text{ cm}^{-2}$. Nevertheless, the observed X-ray luminosity (which can significantly underestimate the intrinsic X-ray power) is too small to drive the observed UV/optical variability. The sight line from the corona to the disk might not be heavily obscured; it is unclear whether the illuminating X-ray is able to induce the observed variations in disk emission or not. Hence, it is interesting to explore the UV/optical cross-correlations in X-ray weak quasars.

So far, the disk mapping is performed for AGNs with low luminosity (thus strong X-ray power) or X-ray normal quasars. If the "lamppost" thermal reprocessing is correct, we expect no inter-band cross-correlations with time delays in the UV/optical light curves of X-ray weak quasars. Hence, X-ray weak quasars are ideal for verifying the X-ray reprocessing and probing alternative possible UV/optical variability mechanisms. Here we report the time delay of the g and r band continua of an X-ray weak quasar, SDSS J153913.47+395423.4 (hereafter SDSS J1539+3954). To our best knowledge, SDSS J1539+3954 has the highest black-hole mass, optical luminosity, and redshift among AGNs with continuum time lag measurements. This manuscript is formatted as follows. In Section 2, we describe the properties of the X-ray weak quasar SDSS J1539+3954. In Section 3, we present our results. In Section 4, we discuss the physical implications of our results. A summary is given in Section 5.

2. SDSS J1539+3954 PROPERTIES

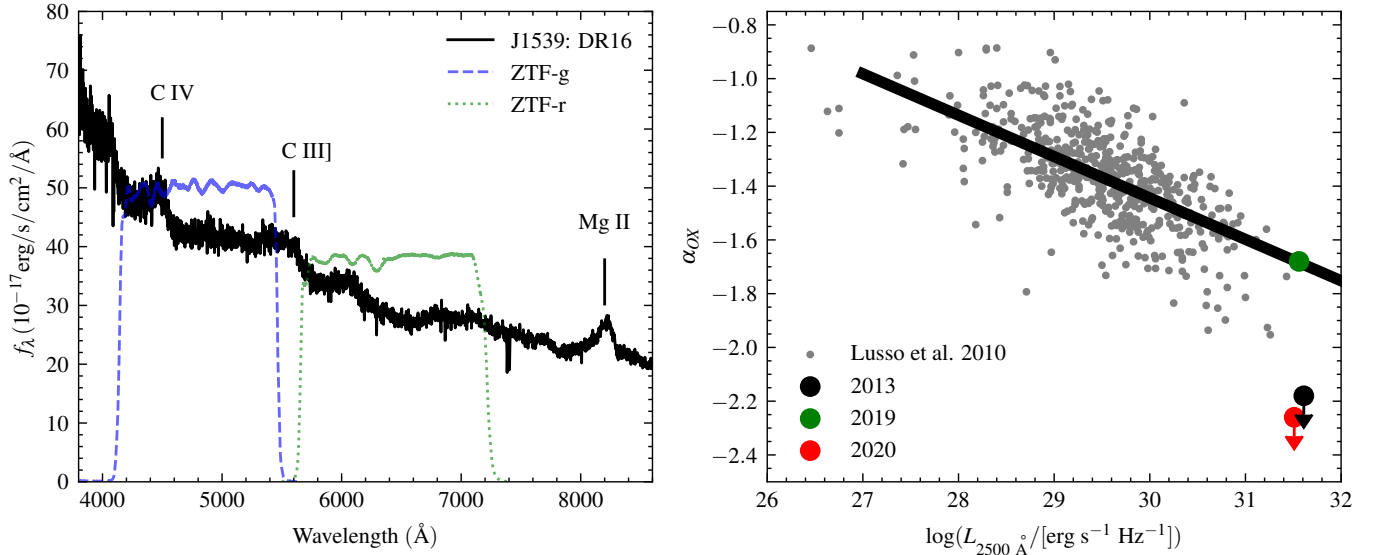


Figure 1. Left panel: The SDSS DR16 spectrum (black curve) of SDSS J1539+3954 and the ZTF g and r filter response curves, in blue and green, respectively. Major broad emission lines, i.e., C IV, C III], and Mg II, are marked. C IV and C III] are exceptionally weak in SDSS J1539+3954. Right panel: The X-ray to UV power-law slope α_{OX} vs. the rest-frame monochromatic luminosity L_{2500} . Grey dots are X-ray-selected type 1 AGN samples by Lusso et al. (2010). The solid line represents the best-fitting line obtained by Lusso et al. (2010). The green point represents the X-ray normal state of our target in 2019, well consistent with the relation of Lusso et al. (2010). Red and black points are the 90% confidence upper limits for our X-ray weak quasar SDSS J1539+3954 (Ni et al. 2020). Its 2013 and 2020 data points are slightly horizontally shifted for better visibility. SDSS J1539+3954 has a significantly lower value of α_{OX} in 2013 and 2020 (Ni et al. 2020) than in typical type 1 sources.

SDSS J1539+3954 lies at redshift 1.935, with J2000 coordinates RA: 234.806121° , DEC: $+39.906525^\circ$, and an i -band apparent magnitude $i = 17.38$ (Adelman-McCarthy et al. 2006). The black-hole mass $\log(M_{\text{BH}}/M_{\odot}) = 9.8$ with the typical uncertainty of 0.4 dex, and the bolometric luminosity $\log(L_{\text{bol}}/[\text{erg s}^{-1}]) = 47.3207 \pm 0.0009$ (Wu & Shen 2022) estimated based on the optical luminosity at rest-frame 3000 Å. Note that this black-hole mass is estimated via the broad Mg II line. We caution, however, that there are caveats associated with the Mg II line-based virial black-hole mass, such as profile complexity, profile shape, spectral noise (e.g., Marziani et al. 2013; Sun et al. 2015; Kovačević-Dojčinović et al. 2017). On the left panel of Fig. 1, we show the SDSS DR16 spectrum (Ahumada et al. 2020) of SDSS J1539+3954 and the ZTF g and r filter response curves. Major broad emission lines, e.g., C IV, C III], and Mg II are marked in the figure. Due to its large redshift, the more reliable $\text{H}\beta$ mass estimator is not covered by the SDSS spectrum.

According to the observed-frame 0.5–2 keV fluxes (Luo et al. 2015; Ni et al. 2020, 2022), the corresponding Galactic absorption-corrected 2–10 keV X-ray luminosities of SDSS J1539+3954 are $\log(L_X/[\text{erg s}^{-1}]) \leq 43.76$, $= 45.04$, and < 44.07 in the 2013, 2019, and 2020 X-ray observations, respectively. Even during the X-ray flare stage (in 2019), SDSS J1539+3954 shows a negligible amount of X-ray power compared to its UV/optical luminosity. SDSS J1539+3954 shows strong variations in α_{OX} (Luo et al. 2015; Ni et al. 2020, 2022). During nearly 7 years, its value went from < -2.18 to -1.68 and back to < -2.26 (X-ray weak) in 2013, 2019, and 2020, respectively (see Fig. 1). Ni et al. (2020) studied the extreme X-ray variability in SDSS J1539+3954 and proposed its nature as being due to a geometrically and optically thick accretion disk whose thickness varies.

We examine SDSS J1539+3954 in two bands (g and r) using the ZTF data. We retrieve the ZTF g , r , and i band light curves of SDSS J1539+3954 via the IRSA GATOR ZTF catalog service¹. ZTF is a time-domain survey with the 1.2 meters Schmidt telescope at the Palomar Observatory (Masci et al. 2019). Each ZTF exposure time is 30 seconds with a 5σ sensitivity limit of 20.8 and 20.6 in the g and r bands, respectively. We use the point spread function (PSF) magnitudes with the "catflags" parameter equal to zero (i.e., good quality data, not affected by clouds and/or the

¹ <https://irsa.ipac.caltech.edu/cgi-bin/Gator>

moon, or instrument; see [Masci et al. 2019](#)). The total time duration of the light curves are: 1564, 1568, and 1043 days, for g , r , and i bands, respectively. The median cadence of each light curve is: 1.50, 0.79, and 3.52 days for g , r , and i bands, respectively. The ZTF's g , r , and i bands light curves, with the best-fitting 2nd order polynomial curves for g and r , are presented in Figure 2. The g and r light curves show prominent variations on short and long timescales. The i -band light curve is sparse and is excluded in the subsequent time lag analysis.

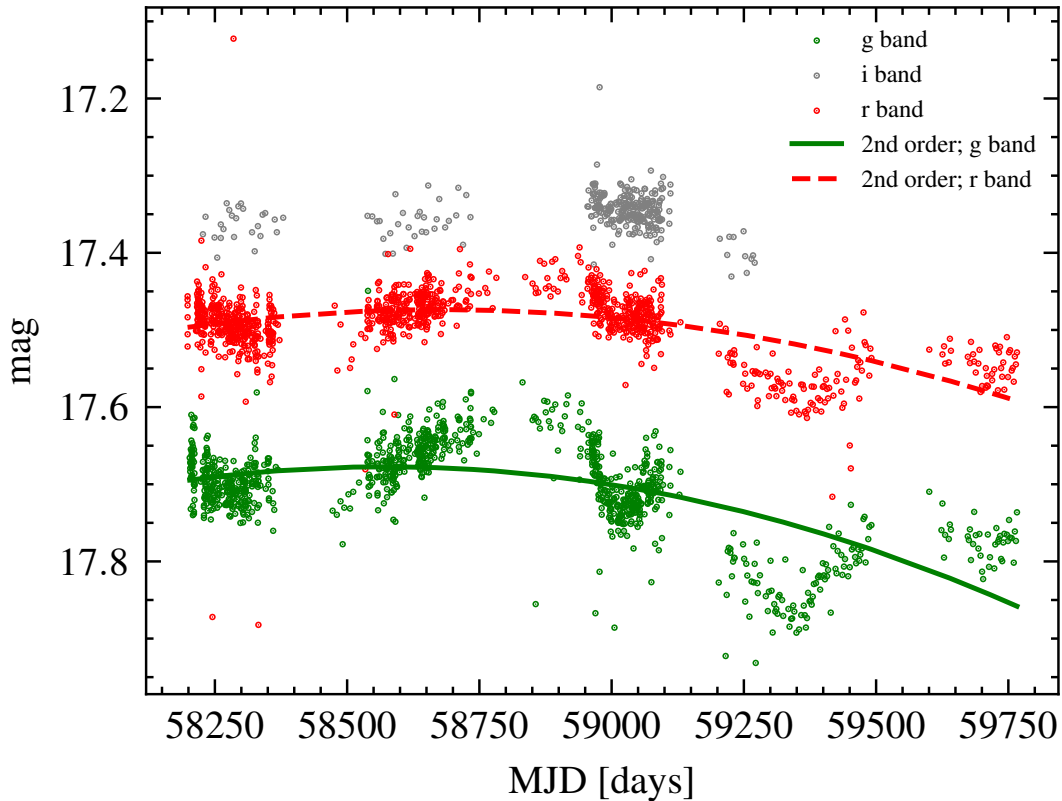


Figure 2. The g , r , and i -band light curves of the SDSS J1539+3954 from ZTF. The green solid and red dashed curves are the best-fitting second-order polynomial curves for g and r , respectively. Due to the limited coverage of the i band, we will not analyze the i -band light curves. For the sake of completeness, we have included it in the plot

3. RESULTS

We measure the cross-correlation and time delay of the ZTF g and r light curves of SDSS J1539+3954 (Fig. 2). To determine the inter-band time lags, we use PyCCF ([Sun et al. 2018](#)), a Python version of the interpolation cross-correlation function code based on [Peterson et al. \(1998\)](#). The light curves used in the PyCCF are from MJD = 58200 days to MJD = 59800 days. The time delay (τ) searching range was from -200 days to 200 days with a 0.2 -day step. The PyCCF code uses the flux randomization/random-subset selection method to estimate the time lag uncertainties.

The cross-correlation analysis can be biased if the long-term trend is not adequately subtracted from the data ([Welsh 1999](#)). Following previous studies (e.g., [Fausnaugh et al. 2016](#)), we adopt the following two steps to detrend the ZTF light curves. First, we fit low-order polynomial functions to the observed light curves via the least squares method. Second, we subtract the best-fitting polynomial functions from the observed light curves. The residuals are used for subsequent cross-correlation analysis. We use both the first and second-order polynomial functions (see curves in Fig. 2). The cross-correlation function of the second-order polynomial approach and the corresponding distribution (obtained via the flux randomization/random-subset selection method) for the time lag between g and r bands ($\tau_{gr,obs}$) in the observed-frame are presented in Fig. 3. The observed-frame time delays and their 1σ uncertainties are 40_{-5}^{+6} days and 33_{-5}^{+6} days, respectively. The two-time delays are statistically consistent with each other within their 1σ

uncertainties (i.e., $\simeq 5$ days). Note that the time delay of the observed ZTF light curves without detrending is 36 ± 5 days (observed-frame), which also statistically agrees with our first and second-order polynomial results. In summary, a significant cross-correlation with a time delay of $\tau_{\text{gr,obs}} \sim 33$ days (observed-frame) is detected in the X-ray weak quasar SDSS J1539+3954.

The theoretical time delay can be calculated for the X-ray reprocessing of the Shakura & Sunyaev disk. We use the black-hole mass and bolometric luminosity from Section 2. Following Eq. 1 in Li et al. (2021), we calculate the expected $\lambda = 2500 \text{ \AA}$ disk lag ($\tau_{2500,\text{th}}$) with respect to the driving light curve, i.e., $\tau_{2500,\text{th}} = 15.8$ days (rest-frame). The theoretical rest-frame time delay between the g and r bands is $\tau_{\text{gr,th}} = \tau_{2500,\text{th}}((\lambda_r/2500)^{4/3} - (\lambda_g/2500)^{4/3}) = 3.8$ days, where $\lambda_g = 4776/(1+z)$ and $\lambda_r = 6231/(1+z)$ are the rest-frame wavelengths of the g and r bands, respectively. Hence, the theoretical time lag in the observed-frame is $\tau_{\text{gr,th}}(1+z) = 11.2$ days, which is smaller than the observed one ($\tau_{\text{gr,obs}} \sim 33$ days) by a factor of three. This larger-than-expected time lag result is observed in many previous studies (e.g., Fausnaugh et al. 2016; Cackett et al. 2018; Edelson et al. 2019; Netzer 2022; Guo, H. et al. 2022; Guo, W.-J. et al. 2022).

Given its large M_{BH} , the observed g and r emission regions of SDSS J1539+3954 are, unlike lower-mass Seyferts, very close to the SMBH. Indeed, according to the Shakura & Sunyaev disk model, the average sizes of the g and r emission regions are $c\tau_{2500,\text{th}}(\lambda_g/2500)^{4/3} = 24 R_g$ and $c\tau_{2500,\text{th}}(\lambda_r/2500)^{4/3} = 35 R_g$, respectively, where $R_g = GM_{\text{BH}}/c^2$. Hence, general-relativistic corrections and inner-boundary effects can be significant when estimating the theoretical time delay. These effects are considered by Kammoun et al. (2021a) and Kammoun et al. (2021b); they provide an analytic prescription of the expected time delay. Based on Kammoun et al. (2021a), we calculated the $g-r$ time lag for our target with the following parameters: $\log(M_{\text{BH}}/M_{\odot}) = 9.8$, the dimensionless accretion rate $\dot{m} = 0.26$ (Wu & Shen 2022), X-ray luminosity $\log(L_X/[\text{erg s}^{-1}]) = 45.04$ (Ni et al. 2020) at normal state, and the corona height is $10 R_g$. Several studies (e.g., Kammoun et al. 2021b) adopt much higher corona heights (e.g., $\sim 100 R_g$) for some sources; in our opinion, the corona height in SDSS J1539+3954 cannot be large; otherwise, the disk would not effectively obscure the X-ray emission. The $g-r$ time lag for the corona height = $10 R_g$ is 17.19 days in the rest-frame. Recently, a new analytical prescription that involves disk color correction is also obtained (priv. comm., Kammoun 2023 et al. in prep.); with a color correction factor of 1.6, the theoretical $g-r$ time lag is (rest-frame) 10.37 days. These results are roughly consistent with our observations.

Note that the virial black-hole mass might be underestimated in weak-line quasars (e.g., Marculewicz & Nikolajuk 2020) and SDSS J1539+3954 is also a weak-line quasar (e.g., Wu et al. 2011, 2012; Plotkin et al. 2015; Luo et al. 2015). If so, the theoretical time lag is also underestimated. We will discuss this in Section 4.

4. DISCUSSION AND PHYSICAL IMPLICATIONS

4.1. The driving mechanism for the UV/optical variability

Our results (i.e., evident cross-correlations with time lags) for SDSS J1539+3954 are unexpected in the X-ray reprocessing model and have important implications for our understanding of the structure of accretion disks and the interplay between accretion disks and coronae. To explain the results, we propose several possibilities.

If the ‘‘lamppost’’ thermal reprocessing is correct, the X-ray luminosity that illuminates the accretion disk should be much stronger than we observed. On 2013-12-13, the 2-10 keV X-ray luminosity was $< 5.72 \times 10^{43} \text{ erg s}^{-1}$. In 2019-09-12 it increased to $1.09 \times 10^{45} \text{ erg s}^{-1}$ and in 2020-06-17 it went back to the low stage of $< 1.17 \times 10^{44} \text{ erg s}^{-1}$ (Ni et al. 2022). Since the observed UV/optical variability amplitude is about 10%, the required X-ray luminosity should be at least 10% of the UV/optical luminosity. In the ‘‘lamppost’’ thermal reprocessing model, the whole disk emission will vary in response to the X-ray. Suppose we assume the variability amplitudes of the disk emission in other bands (which is not probed by ZTF) are also around 10%. We can conclude that the required X-ray power should be at least 10% of the bolometric luminosity. The bolometric luminosity is $2.09 \times 10^{47} \text{ erg s}^{-1}$ which indicates that the required X-ray power is $\sim 2.09 \times 10^{46} \text{ erg s}^{-1}$. Hence, the required X-ray power is at least 19 times larger than the observed one (2019). An even higher value of X-ray power (a factor of ≥ 178) is required for the 2020 X-ray observation.

We present two possible solutions: i) the X-ray emission is extremely anisotropic. ii) the ambient gas may act as a ‘‘shielding’’ gas and blocks most of the X-ray photons. Hence, the intrinsic corona is strong, but the observed X-ray weakness could be caused by dust-free gas absorption (Wang et al. 2022), which might be related to the disk winds. Note that the X-ray spectrum of the *CHANDRA* observation in 2019 has a typical quasar photon index of $\Gamma = 2$ (Ni et al. 2020), i.e., no significant intrinsic absorption. Hence, the observed X-ray luminosity is the same as the intrinsic one. Even in this case, the X-ray emission is not powerful enough to drive the variability in the disk

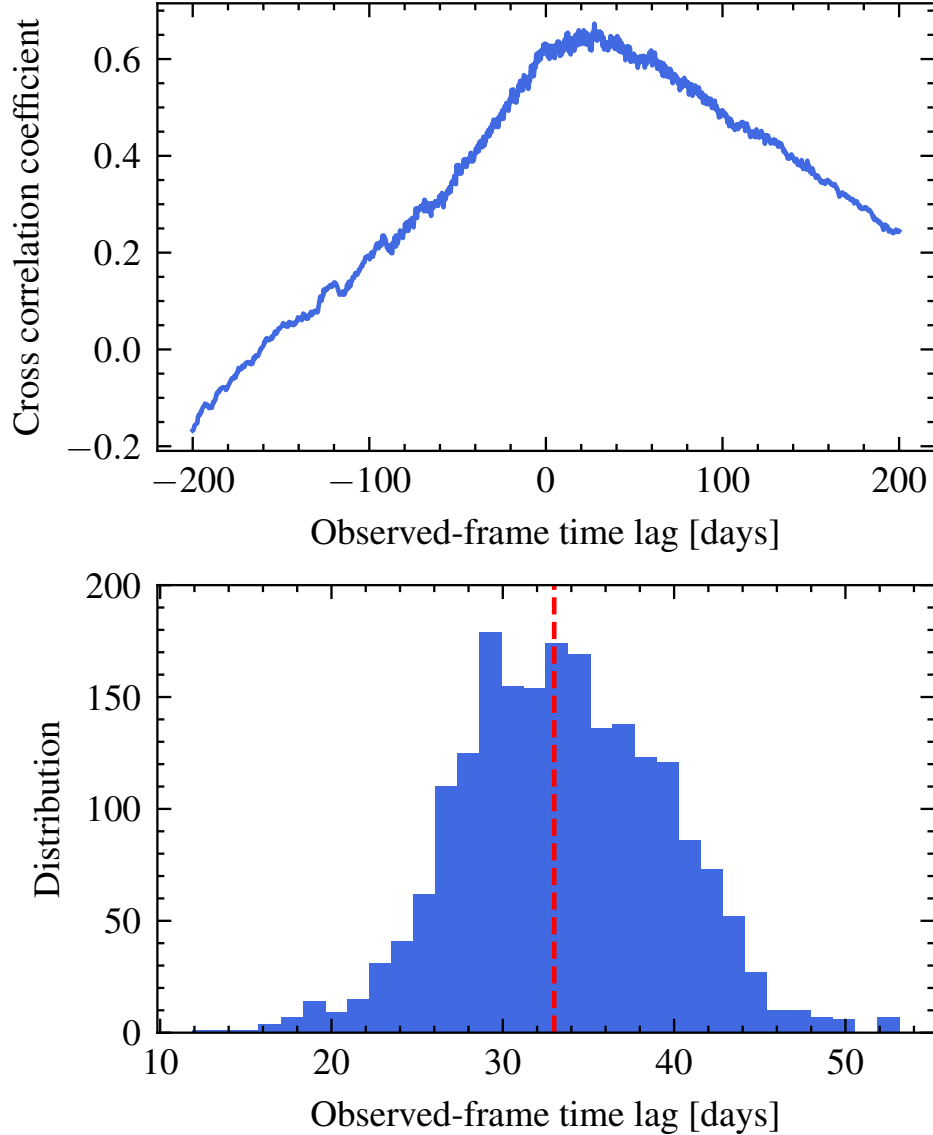


Figure 3. Top panel: The observed-frame time lag between g and r bands in days vs. correlation coefficient for the 2nd-order polynomial approach. This approach is based on subtracting the 2nd-order polynomial linear least-squares fit (with equal weight given to all data points) from the original light curves. Bottom panel: The g -vs- r time delay ($\tau_{gr,obs}$) centroid distribution (from the flux randomization/random-subset selection method) for the 2nd-order polynomial approach. The red dashed line indicates the median value.

emission. If the “lamppost” thermal reprocessing model is incorrect, some alternative explanations are proposed (e.g., Li et al. 2021, and references therein). First, we consider the disk-corona magnetic coupling scenario, also known as the CHAR model (Sun et al. 2020). In this model, strong magnetic fluctuations in the corona rather than the X-ray illumination induce the variations in the disk and produce the multi-band correlated variations with time delays (for a more detailed discussion, please see Sun et al. 2020). The corresponding time lags are not light-travel time delays. For luminous quasars like J1539, the time delay of the CHAR model without general-relativistic effects is similar to $\tau_{gr,th}$ (see Li et al. 2021). However, we caution that the general-relativistic CHAR model is still under development and a detailed comparison to our results is beyond the scope of this work. Second, our results can be understood in the EUV reprocessing model. In this model, it is the EUV emission coming from the innermost “EUV region” rather than the X-ray that illuminates the outer disk (Gardner & Done 2017) and drives the UV/optical variability. A puffed thick disk, which is widely proposed to form in X-ray weak quasars, might act as the “EUV torus”. Future determination

of the rest-frame UV/optical time lag-wavelength relation of SDSS J1539+3954 (via, e.g., LCOGT) can test these mechanisms.

4.2. The scaling relation between inter-band time lags and luminosities

Study of SDSS J1539+3954 allows us to extend the continuum emission radius-luminosity relation at 5100 Å to the high-luminosity end. In fact, SDSS J1539+3954 is almost one order of magnitude more luminous than the most luminous quasars in previous time lag-luminosity studies (Guo, H. et al. 2022; Netzer 2022; Montano et al. 2022). To obtain the radius at 5100 Å (R_{5100}^{rest}) from the time lag, we assume that $R_\lambda \propto \lambda^{4/3}$ (Guo, H. et al. 2022). Hence, we expect that

$$R_{5100}^{\text{rest}} = \frac{\tau_{\text{gr,obs}}/(1+z)}{(\lambda_r/5100)^{4/3} - (\lambda_g/5100)^{4/3}} = 120 \pm 18 \text{ (lt - days)}, \quad (1)$$

where $\tau_{\text{gr,obs}}$, λ_g , and λ_r are defined in Sec. 3. We also include the “core” sample and local AGNs of Guo, H. et al. (2022) for subsequent analysis.

To estimate L_{5100} of SDSS J1539+3954, we use the same L_{bol} as in Sec. 2 (which was estimated from L_{3000} ; see Sec. 4.1 of Wu & Shen 2022), and the L_{5100} bolometric factor of 10 (Richards et al. 2006), i.e., $L_{5100} = L_{\text{bol}}/10$. Following Guo, H. et al. (2022), we assumed the same uncertainty, i.e., 0.05 dex. Hence, $\log(L_{5100}/[\text{erg s}^{-1}]) = 46.32 \pm 0.05$.

We assume the scaling relation between R_{5100} and L_{5100} follows

$$\log(R_{5100}/[\text{lt - days}]) = m \log(L_{5100}/[\text{erg s}^{-1}]) + b, \quad (2)$$

where m and b are the slope and intercept of the relation. We fit Eq. 2 to SDSS J1539+3954, the “core” sample, and the local AGN sample in Guo, H. et al. (2022). We adopt the maximum likelihood approach and use MCMC (via emcee) to sample the following likelihood (Hogg et al. 2010),

$$\mathcal{L} = -\frac{1}{2} \sum_n \left[\frac{(\log(R_{5100}^{\text{rest}}/[\text{lt - days}]) - m \log(L_{5100}/[\text{erg s}^{-1}]) - b)^2}{s_n^2} + \ln(2\pi s_n^2) \right], \quad (3)$$

where

$$s_n^2 = (\delta \log(R_{5100}^{\text{rest}}/[\text{lt - days}]))^2 + f^2(m \log(L_{5100}/[\text{erg s}^{-1}]) + b)^2, \quad (4)$$

and $\delta \log(R_{5100}^{\text{rest}}/[\text{lt - days}])$ and f are the measurement error of $\log(R_{5100}^{\text{rest}}/[\text{lt - days}])$ and the intrinsic scatter factor, respectively.

From the MCMC chains, we find the median values of m and b and their 1σ uncertainties. Our fitting results are $m = 0.52 \pm 0.03$ and $b = -22_{-1.4}^{+1.4}$. The best-fitting result, which is shown in Figure 4, is statistically consistent with Guo, H. et al. (2022) and Netzer (2022). Note that our target is not included in their fitting process.

Unlike other sources, SDSS J1539+3954 is a weak-line quasar. As a result, the diffuse continuum from the inner BLR clouds should also be weak since its emission regions are smaller than the $\text{H}\beta$ emission regions by a factor of eight (Netzer 2022), i.e., comparable to the emission regions for high-ionization lines. Hence, if the diffuse continuum is responsible for the scaling relation between R_{5100} and L_{5100} (as proposed by Netzer 2022), we expect that SDSS J1539+3954 lies below the scaling relation. This expectation is inconsistent with the data. Hence, our results indicate that the diffuse continuum might not be the only mechanism to produce the scaling relation between R_{5100} and L_{5100} .

We now discuss the impacts of the virial black-hole mass estimations. Recently, Marculewicz & Nikolajuk (2020) adopt the continuum fitting method (e.g., Castignani et al. 2013; Capellupo et al. 2015) to estimate M_{BH} in WLQs. Comparing with our SED fitting M_{BH} , the virial black-hole mass based on $\text{H}\beta$ is systematically smaller by an average factor of four to five. If the Mg II-based virial mass of SDSS J1539+3954 is similarly smaller than the actual M_{BH} by a factor of ~ 4 , we expect that the theoretical time lags in Section 3 should increase by a factor of $\sim 4^{1/3} = 1.5$, i.e., this mass discrepancy still cannot account for the difference between the theoretical and observed time lags.

5. CONCLUSION

In this study, we use ZTF observations to explore the inter-band time lag between g and r for an X-ray weak quasar, SDSS J1539+3954. Our main findings can be summarized as follows. First, a significant cross-correlation with a time delay of $\tau_{\text{gr,obs}} = 33_{-5}^{+6}$ days (observed-frame) is detected. Our observed time delay is about three times

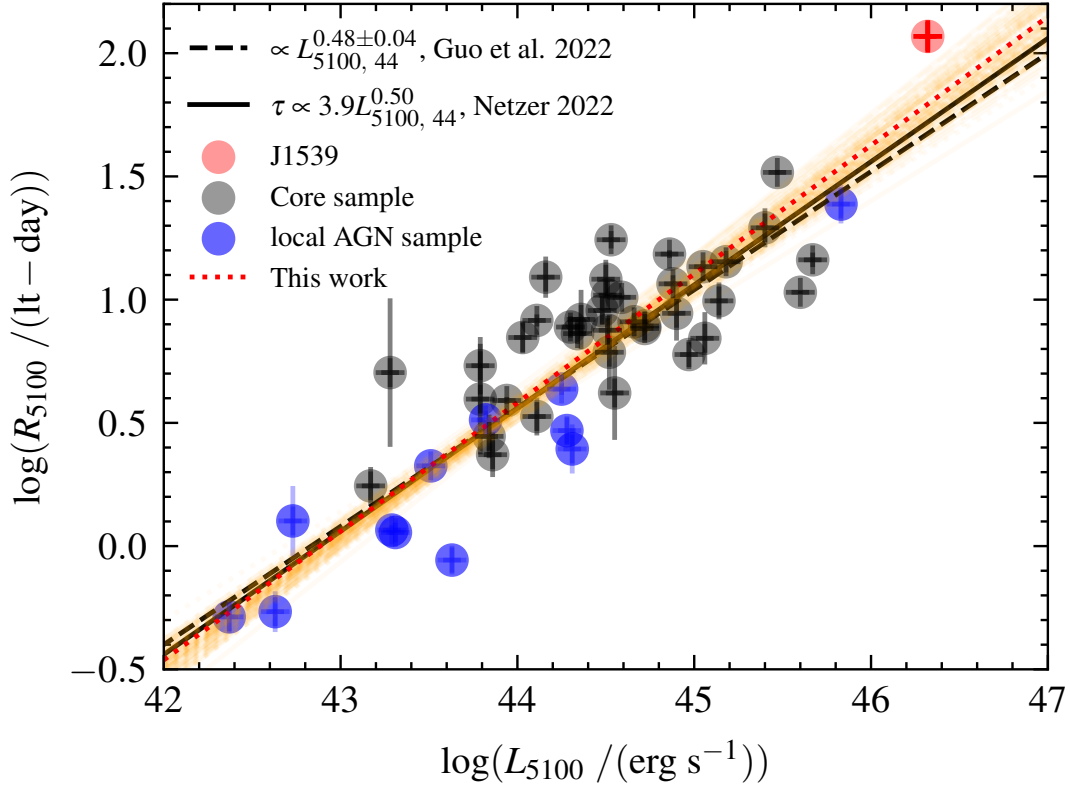


Figure 4. The radius-luminosity relation at 5100 Å. The best linear fit (red dotted line) applies to all sources with a typical luminosity uncertainty of 0.05 dex. The black solid and dashed lines correspond to the relations in [Netzer \(2022\)](#) and [Guo, H. et al. \(2022\)](#). SDSS J1539+3954 helps to extend the radius-luminosity relation to the higher end of L_{5100} . Given its weak-line nature, one would expect that SDSS J1539+3954 falls below the radius-luminosity relation if the diffuse continuum is the only mechanism that accounted for this relation. This expectation is inconsistent with our observation.

larger than the X-ray reprocessing in a Shakura & Sunyaev disk if the virial black-hole mass is valid and if the lag is dominated by a simple light-travel time. The X-ray reprocessing in a general-relativistic disk can account for the observed time lag. Second, to understand the observed time delay, the X-ray power of SDSS J1539+3954 should be at least 19 times larger than the X-ray observations. Such inconsistency in the “lamppost” thermal reprocessing model is possible if: a. the corona emission is anisotropic; b. strong absorption is present (e.g., by winds). Alternatively, we argue that the magnetic coupling scenario ([Sun et al. 2020](#)) or the EUV reprocessing model can explain our results ([Gardner & Done 2017](#)). Additionally, due to the high luminosity of SDSS J1539+3954, we were able to extend the range of the radius-luminosity relation (see Fig. 4). We obtained $R_{5100}^{\text{rest}} = 120 \pm 18$ (lt - days) which lies slightly above the R_{5100}^{rest} -luminosity relation of [Netzer \(2022\)](#). This relation is proposed to be driven by the diffuse continuum from the BLR. The diffuse continuum is rather weak in SDSS J1539+3954 since this source is a weak emission-line quasar. Hence, we would expect that SDSS J1539+3954 lies below the R_{5100}^{rest} -luminosity relation. The inconsistency between our observation and expectation suggests that other/additional mechanisms (e.g., the CHAR model) could also contribute to the R_{5100}^{rest} -luminosity relation. Further investigation of the inter-band time lags in other X-ray weak AGNs will bring opportunities to understand the physical origin of quasar UV/optical variability, inter-band time lags, and disk sizes.

ACKNOWLEDGEMENTS

1 We would like to thank the anonymous referee for useful comments that improved the clarity of the paper. M.M. and
 2 M.Y.S. would like to thank Bin Luo for the valuable discussion. M.M. would like to thank Elias Kammoun for the
 3 valuable discussion. M.Y.S. acknowledges support from the National Natural Science Foundation of China (NSFC-
 4 11973002), the Natural Science Foundation of Fujian Province of China (No. 2022J06002), and the China Manned
 5 Space Project grants (No. CMS-CSST-2021-A06; No. CMS-CSST-2021-B11). J.W. acknowledges support from the
 6 National Natural Science Foundation of China (NSFC-12273029 and NSFC-12221003), and the China Manned Space
 7 Project grants (No. CMS-CSST-2021-A05; No. CMS-CSST-2021-A06). Z.X.Z. acknowledges support from the National
 8 Natural Science Foundation of China (NSFC-12033006 and NSFC-12103041).

9 Based on observations obtained with the Samuel Oschin Telescope 48-inch and the 60-inch Telescope at the Palomar
 10 Observatory as part of the Zwicky Transient Facility project. ZTF is supported by the National Science Foundation
 11 under Grants No. AST-1440341 and AST-2034437 and a collaboration including current partners Caltech, IPAC,
 12 the Weizmann Institute for Science, the Oskar Klein Center at Stockholm University, the University of Maryland,
 13 Deutsches Elektronen-Synchrotron and Humboldt University, the TANGO Consortium of Taiwan, the University of
 14 Wisconsin at Milwaukee, Trinity College Dublin, Lawrence Livermore National Laboratories, IN2P3, University of
 15 Warwick, Ruhr University Bochum, Northwestern University and former partners the University of Washington, Los
 16 Alamos National Laboratories, and Lawrence Berkeley National Laboratories. Operations are conducted by COO,
 17 IPAC, and UW.

Facilities: ZTF (IRSA 2022)

Software: astropy (Astropy Collaboration et al. 2018), matplotlib (Hunter 2007), numpy (van der Walt et al. 2011), PyCCF (Sun et al. 2018), emcee (Foreman-Mackey et al. 2013).

REFERENCES

- Adelman-McCarthy, J. K., Agüeros, M. A., Allam, S. S.,
 et al. 2006, ApJS, 162, 38, doi: [10.1086/497917](https://doi.org/10.1086/497917)
- Ahumada, R., Allende Prieto, C., Almeida, A., et al. 2020,
 ApJS, 249, 3, doi: [10.3847/1538-4365/ab929e](https://doi.org/10.3847/1538-4365/ab929e)
- Arévalo, P., Uttley, P., Kaspi, S., et al. 2008, MNRAS, 389,
 1479, doi: [10.1111/j.1365-2966.2008.13719.x](https://doi.org/10.1111/j.1365-2966.2008.13719.x)
- Astropy Collaboration, Price-Whelan, A. M., Sipőcz, B. M.,
 et al. 2018, AJ, 156, 123, doi: [10.3847/1538-3881/aabc4f](https://doi.org/10.3847/1538-3881/aabc4f)
- Cackett, E. M., Bentz, M. C., & Kara, E. 2021, iScience,
 24, 102557, doi: [10.1016/j.isci.2021.102557](https://doi.org/10.1016/j.isci.2021.102557)
- Cackett, E. M., Chiang, C.-Y., McHardy, I., et al. 2018,
 ApJ, 857, 53, doi: [10.3847/1538-4357/aab4f7](https://doi.org/10.3847/1538-4357/aab4f7)
- Cackett, E. M., Horne, K., & Winkler, H. 2007, MNRAS,
 380, 669, doi: [10.1111/j.1365-2966.2007.12098.x](https://doi.org/10.1111/j.1365-2966.2007.12098.x)
- Cackett, E. M., Gelbord, J., Li, Y.-R., et al. 2020, ApJ,
 896, 1, doi: [10.3847/1538-4357/ab91b5](https://doi.org/10.3847/1538-4357/ab91b5)
- Cai, Z.-Y., Wang, J.-X., Zhu, F.-F., et al. 2018, ApJ, 855,
 117, doi: [10.3847/1538-4357/aab091](https://doi.org/10.3847/1538-4357/aab091)
- Capellupo, D. M., Netzer, H., Lira, P., Trakhtenbrot, B., &
 Mejía-Restrepo, J. 2015, MNRAS, 446, 3427,
 doi: [10.1093/mnras/stu2266](https://doi.org/10.1093/mnras/stu2266)
- Castignani, G., Haardt, F., Lapi, A., et al. 2013, A&A, 560,
 A28, doi: [10.1051/0004-6361/201321424](https://doi.org/10.1051/0004-6361/201321424)
- Clavel, J., Nandra, K., Makino, F., et al. 1992, ApJ, 393,
 113, doi: [10.1086/171490](https://doi.org/10.1086/171490)
- Dexter, J., Xin, S., Shen, Y., et al. 2019, ApJ, 885, 44,
 doi: [10.3847/1538-4357/ab4354](https://doi.org/10.3847/1538-4357/ab4354)
- Diamond-Stanic, A. M., Fan, X., Brandt, W. N., et al.
 2009, ApJ, 699, 782, doi: [10.1088/0004-637X/699/1/782](https://doi.org/10.1088/0004-637X/699/1/782)
- Edelson, R., Gelbord, J., Cackett, E., et al. 2019, ApJ, 870,
 123, doi: [10.3847/1538-4357/aaf3b4](https://doi.org/10.3847/1538-4357/aaf3b4)
- Fausnaugh, M. M., Denney, K. D., Barth, A. J., et al. 2016,
 ApJ, 821, 56, doi: [10.3847/0004-637X/821/1/56](https://doi.org/10.3847/0004-637X/821/1/56)
- Foreman-Mackey, D., Hogg, D. W., Lang, D., & Goodman,
 J. 2013, PASP, 125, 306, doi: [10.1086/670067](https://doi.org/10.1086/670067)
- Gardner, E., & Done, C. 2017, MNRAS, 470, 3591,
 doi: [10.1093/mnras/stx946](https://doi.org/10.1093/mnras/stx946)
- Gibson, R. R., Brandt, W. N., & Schneider, D. P. 2008,
 ApJ, 685, 773, doi: [10.1086/590403](https://doi.org/10.1086/590403)
- Guo, H., Barth, A. J., & Wang, S. 2022, ApJ, 940, 20,
 doi: [10.3847/1538-4357/ac96ec](https://doi.org/10.3847/1538-4357/ac96ec)
- Guo, W.-J., Li, Y.-R., Zhang, Z.-X., Ho, L. C., & Wang,
 J.-M. 2022, ApJ, 929, 19, doi: [10.3847/1538-4357/ac4e84](https://doi.org/10.3847/1538-4357/ac4e84)
- Hall, P. B., Sarrouh, G. T., & Horne, K. 2018, ApJ, 854,
 93, doi: [10.3847/1538-4357/aaa768](https://doi.org/10.3847/1538-4357/aaa768)
- Hogg, D. W., Bovy, J., & Lang, D. 2010, arXiv e-prints,
 arXiv:1008.4686, doi: [10.48550/arXiv.1008.4686](https://doi.org/10.48550/arXiv.1008.4686)

- Homayouni, Y., Trump, J. R., Grier, C. J., et al. 2019, *ApJ*, 880, 126, doi: [10.3847/1538-4357/ab2638](https://doi.org/10.3847/1538-4357/ab2638)
- Hunter, J. D. 2007, *Computing in Science and Engineering*, 9, 90, doi: [10.1109/MCSE.2007.55](https://doi.org/10.1109/MCSE.2007.55)
- IRSA. 2022, Zwicky Transient Facility Image Service, IPAC, doi: [10.26131/IRSA539](https://doi.org/10.26131/IRSA539)
- Just, D. W., Brandt, W. N., Shemmer, O., et al. 2007, *ApJ*, 665, 1004, doi: [10.1086/519990](https://doi.org/10.1086/519990)
- Kammoun, E. S., Dovčiak, M., Papadakis, I. E., Caballero-García, M. D., & Karas, V. 2021a, *ApJ*, 907, 20, doi: [10.3847/1538-4357/abcb93](https://doi.org/10.3847/1538-4357/abcb93)
- Kammoun, E. S., Papadakis, I. E., & Dovčiak, M. 2021b, *MNRAS*, 503, 4163, doi: [10.1093/mnras/stab725](https://doi.org/10.1093/mnras/stab725)
- Korista, K. T., & Goad, M. R. 2019, *MNRAS*, 489, 5284, doi: [10.1093/mnras/stz2330](https://doi.org/10.1093/mnras/stz2330)
- Kovačević-Dojčinović, J., Marčeta-Mandić, S., & Popović, L. Č. 2017, *Frontiers in Astronomy and Space Sciences*, 4, 7, doi: [10.3389/fspas.2017.00007](https://doi.org/10.3389/fspas.2017.00007)
- Krolik, J. H., Horne, K., Kallman, T. R., et al. 1991, *ApJ*, 371, 541, doi: [10.1086/169918](https://doi.org/10.1086/169918)
- Li, T., Sun, M., Xu, X., et al. 2021, *ApJL*, 912, L29, doi: [10.3847/2041-8213/abf9aa](https://doi.org/10.3847/2041-8213/abf9aa)
- Luo, B., Brandt, W. N., Hall, P. B., et al. 2015, *ApJ*, 805, 122, doi: [10.1088/0004-637X/805/2/122](https://doi.org/10.1088/0004-637X/805/2/122)
- Lusso, E., Comastri, A., Vignali, C., et al. 2010, *A&A*, 512, A34, doi: [10.1051/0004-6361/200913298](https://doi.org/10.1051/0004-6361/200913298)
- Marculewicz, M., & Nikolažuk, M. 2020, *ApJ*, 897, 117, doi: [10.3847/1538-4357/ab9597](https://doi.org/10.3847/1538-4357/ab9597)
- Marlar, A., Shemmer, O., Anderson, S. F., et al. 2018, *ApJ*, 865, 92, doi: [10.3847/1538-4357/aad812](https://doi.org/10.3847/1538-4357/aad812)
- Marziani, P., Sulentic, J. W., Plauchu-Frayn, I., & del Olmo, A. 2013, *A&A*, 555, A89, doi: [10.1051/0004-6361/201321374](https://doi.org/10.1051/0004-6361/201321374)
- Masci, F. J., Laher, R. R., Rusholme, B., et al. 2019, *PASP*, 131, 018003, doi: [10.1088/1538-3873/aae8ac](https://doi.org/10.1088/1538-3873/aae8ac)
- McHardy, I. M., Connolly, S. D., Horne, K., et al. 2018, *MNRAS*, 480, 2881, doi: [10.1093/mnras/sty1983](https://doi.org/10.1093/mnras/sty1983)
- Miniutti, G., Brandt, W. N., Schneider, D. P., et al. 2012, *MNRAS*, 425, 1718, doi: [10.1111/j.1365-2966.2012.21648.x](https://doi.org/10.1111/j.1365-2966.2012.21648.x)
- Montano, J. W., Guo, H., Barth, A. J., et al. 2022, *ApJL*, 934, L37, doi: [10.3847/2041-8213/ac7e54](https://doi.org/10.3847/2041-8213/ac7e54)
- Murray, N., Chiang, J., Grossman, S. A., & Voit, G. M. 1995, *ApJ*, 451, 498, doi: [10.1086/176238](https://doi.org/10.1086/176238)
- Netzer, H. 2022, *MNRAS*, 509, 2637, doi: [10.1093/mnras/stab3133](https://doi.org/10.1093/mnras/stab3133)
- Ni, Q., Brandt, W. N., Luo, B., et al. 2018, *MNRAS*, 480, 5184, doi: [10.1093/mnras/sty1989](https://doi.org/10.1093/mnras/sty1989)
- Ni, Q., Brandt, W. N., Yi, W., et al. 2020, *ApJL*, 889, L37, doi: [10.3847/2041-8213/ab6d78](https://doi.org/10.3847/2041-8213/ab6d78)
- Ni, Q., Brandt, W. N., Luo, B., et al. 2022, *MNRAS*, 511, 5251, doi: [10.1093/mnras/stac394](https://doi.org/10.1093/mnras/stac394)
- Peterson, B. M., Wanders, I., Horne, K., et al. 1998, *PASP*, 110, 660, doi: [10.1086/316177](https://doi.org/10.1086/316177)
- Plotkin, R. M., Shemmer, O., Trakhtenbrot, B., et al. 2015, *ApJ*, 805, 123, doi: [10.1088/0004-637X/805/2/123](https://doi.org/10.1088/0004-637X/805/2/123)
- Proga, D., Stone, J. M., & Kallman, T. R. 2000, *ApJ*, 543, 686, doi: [10.1086/317154](https://doi.org/10.1086/317154)
- Richards, G. T., Strauss, M. A., Fan, X., et al. 2006, *AJ*, 131, 2766, doi: [10.1086/503559](https://doi.org/10.1086/503559)
- Shakura, N. I., & Sunyaev, R. A. 1973, *A&A*, 500, 33
- Starkey, D. A., Huang, J., Horne, K., & Lin, D. N. C. 2023, *MNRAS*, 519, 2754, doi: [10.1093/mnras/stac3579](https://doi.org/10.1093/mnras/stac3579)
- Sun, M., Grier, C. J., & Peterson, B. M. 2018, *PyCCF: Python Cross Correlation Function for reverberation mapping studies*, Astrophysics Source Code Library, record ascl:1805.032. <http://ascl.net/1805.032>
- Sun, M., Xue, Y., Trump, J. R., & Gu, W.-M. 2019, *MNRAS*, 482, 2788, doi: [10.1093/mnras/sty2885](https://doi.org/10.1093/mnras/sty2885)
- Sun, M., Trump, J. R., Shen, Y., et al. 2015, *ApJ*, 811, 42, doi: [10.1088/0004-637X/811/1/42](https://doi.org/10.1088/0004-637X/811/1/42)
- Sun, M., Xue, Y., Brandt, W. N., et al. 2020, *ApJ*, 891, 178, doi: [10.3847/1538-4357/ab789e](https://doi.org/10.3847/1538-4357/ab789e)
- Tananbaum, H., Avni, Y., Branduardi, G., et al. 1979, *ApJL*, 234, L9, doi: [10.1086/183100](https://doi.org/10.1086/183100)
- Timlin, J. D., Brandt, W. N., Ni, Q., et al. 2020, *MNRAS*, 492, 719, doi: [10.1093/mnras/stz3433](https://doi.org/10.1093/mnras/stz3433)
- Uttley, P., Edelson, R., McHardy, I. M., Peterson, B. M., & Markowitz, A. 2003, *ApJL*, 584, L53, doi: [10.1086/373887](https://doi.org/10.1086/373887)
- van der Walt, S., Colbert, S. C., & Varoquaux, G. 2011, *Computing in Science and Engineering*, 13, 22, doi: [10.1109/MCSE.2011.37](https://doi.org/10.1109/MCSE.2011.37)
- Wang, C., Luo, B., Brandt, W. N., et al. 2022, *ApJ*, 936, 95, doi: [10.3847/1538-4357/ac886e](https://doi.org/10.3847/1538-4357/ac886e)
- Welsh, W. F. 1999, *PASP*, 111, 1347, doi: [10.1086/316457](https://doi.org/10.1086/316457)
- Wu, J., Brandt, W. N., Anderson, S. F., et al. 2012, *ApJ*, 747, 10, doi: [10.1088/0004-637X/747/1/10](https://doi.org/10.1088/0004-637X/747/1/10)
- Wu, J., Brandt, W. N., Hall, P. B., et al. 2011, *ApJ*, 736, 28, doi: [10.1088/0004-637X/736/1/28](https://doi.org/10.1088/0004-637X/736/1/28)
- Wu, Q., & Shen, Y. 2022, *ApJS*, 263, 42, doi: [10.3847/1538-4365/ac9ead](https://doi.org/10.3847/1538-4365/ac9ead)